

A Non-Nested Multilevel Method for Meshless Solution of the Poisson Equation in Heat Transfer and Fluid Flow

Anand Radhakrishnan, Michael Xu, Shantanu Shahane, Surya Pratap Vanka¹

*Department of Mechanical Science and Engineering
University of Illinois at Urbana-Champaign
Urbana, Illinois 61801*

Abstract

We present a non-nested multilevel algorithm for solving the Poisson equation discretized at scattered points using polyharmonic radial basis function (PHS-RBF) interpolations. We append polynomials to the radial basis functions to achieve exponential convergence of discretization errors. The interpolations are performed over local clouds of points and the Poisson equation is collocated at each of the scattered points, resulting in a sparse set of discrete equations for the unknown variables. To solve this set of equations, we have developed a non-nested multilevel algorithm utilizing multiple independently generated coarse sets of points. The restriction and prolongation operators are also constructed with the same RBF interpolations procedure. The performance of the algorithm for Dirichlet and all-Neumann boundary conditions is evaluated in three model geometries using a manufactured solution. For Dirichlet boundary conditions, rapid convergence is observed

¹Corresponding Author Email: spvanka@illinois.edu

using SOR point solver as the relaxation scheme. For cases of all-Neumann boundary conditions, convergence is seen to slow down with the degree of the appended polynomial. However, when the multilevel procedure is combined with a GMRES algorithm, the convergence is seen to significantly improve. The GMRES accelerated multilevel algorithm is included in a fractional step method to solve incompressible Navier-Stokes equations.

Keywords: Meshless method, Multilevel Method, Radial Basis Function based Finite Difference, Polyharmonic Spline, Poisson Equation

1. Introduction

Multilevel methods[1–5] have been extensively demonstrated to provide optimal iterative convergence of discretized elliptic partial differential equations such as the Poisson equation encountered in numerous engineering problems [6–10]. By restricting residuals from fine to coarse levels, solving them on coarser levels, and prolongating corrections to the finer levels, multilevel methods provide optimal smoothing of all error frequencies encountered in an iterative solution process. The traditional multilevel method [1] uses nested refinement in which a finer grid is generated by subdividing a coarser grid. The refinement can be successively performed until the desired mesh fineness is obtained. For such grids it is very easy to perform restriction and prolongation operations through distance-based interpolations. However, if an arbitrary fine grid is first generated, then the coarsening cannot be performed by a nested procedure. In such a case, several fine grid cells (finite volumes) can be combined to make a coarser cell. Such ‘agglomeration’ multilevel procedures have been developed for Poisson equation [11, 12], for Euler [13–15],

and Navier-Stokes [16–18] equations governing fluid flows. A similar technique is also implemented under the name Additive Correction Multigrid (ACM) [19, 20] in which uniform corrections to the fine grid variables are obtained by solving correction equations on coarser grids generated by combining cells. A more general technique for arbitrary sets of linear equations is the Algebraic Multigrid (AMG) method pioneered by Brandt [21, 22] and implemented as black-box multigrid software [23, 24]. The algebraic multigrid technique coarsens the equation system by examining the strengths of the coefficients, and hence results in efficient coarsening strategies consistent with point iterative solvers. Lastly, non-nested multigrid techniques [25–27] have also been developed as alternatives to agglomeration and additive correction multigrid methods. The advantage of non-nested multigrid methods is that the discretization operator on coarser levels can be constructed directly by the governing equation (as in nested grids), and therefore the multigrid convergence can be optimal. However, because the grids are not nested, several independent grids need to be generated with restriction/prolongation operators constructed from multi-dimensional interpolation formulae. Recently, Katz and Jameson [28] used multiquadrics to discretize the compressible flow equations and accelerated the convergence to steady state by a multi-level meshless method. The coarse sets in their method were generated by a special coarsening algorithm.

The principal characteristic of a multigrid technique is grid-independent rate of convergence of an iterative solver for any arbitrary size of the discrete problem. The number of iterations to reach a specified level of convergence depends only on the rate of convergence of the low frequency errors on the

coarsest level. This is a significant advantage of multigrid based numerical algorithms for elliptic problems. Multigrid methods can also be considered as preconditioners to iterative solvers [29–33], lowering the condition number of the iteration matrix to achieve fast convergence. Multigrid methods have been used for solving sets of coupled equations such as those of fluid flow employing either decoupled or coupled solution of the Navier-Stokes equations [34–38]. For external flows on unstructured grids, agglomeration multigrid with Runge-Kutta time marching schemes have been developed [39].

A recent trend in discretizing partial differential equations in complex domains has been the concept of meshless techniques that use scattered points to represent a complex domain [40–49]. In such meshless methods, a variable is first interpolated either globally [41] or locally over a “cloud” [42] of nearby scattered points using weighted sums of a basis function. The variable is subsequently collocated at the scattered points to evaluate the interpolation coefficients. If the values of any variable are known at the scattered points, the interpolation can then be used to calculate values at in-between locations within the cloud. However, if the values are unknown but satisfy an underlying differential equation, the governing equation can be satisfied discretely at the scattered points either by collocation or by the method of weighted residuals [50–54]. The resulting set of linear (or nonlinear) equations is then solved for the unknown values of the dependent variable at the scattered points.

Some of the common RBFs previously considered for solution of partial

differential equations are as follows:

$$\begin{aligned}
&\text{Multiquadrics (MQ): } \phi(\mathbf{r}) = (\mathbf{r}^2 + c^2)^{1/2} \\
&\text{Inverse Multiquadrics (IMQ): } \phi(\mathbf{r}) = (\mathbf{r}^2 + c^2)^{-1/2} \\
&\text{Gaussian: } \phi(\mathbf{r}) = \exp\left(\frac{-\mathbf{r}^2}{\sigma^2}\right) \\
&\text{Polyharmonic Splines (PHS): } \phi(\mathbf{r}) = \mathbf{r}^{2a+1}, \quad a \in \mathbb{N} \\
&\text{Thin Plate Splines (TPS): } \phi(\mathbf{r}) = \mathbf{r}^{2a} \log(\mathbf{r}), \quad a \in \mathbb{N}
\end{aligned} \tag{1}$$

where r is the magnitude of the distance between two points. The first three radial basis functions need specification of a shape factor c or σ which controls the shape of the RBF. A variable $f(\mathbf{x})$ is interpolated as:

$$f(\mathbf{x}) = \sum_{i=1}^N \alpha_i \phi(\|\mathbf{x} - \mathbf{x}_i\|_2) \tag{2}$$

where the symbol N denotes the number of points used in the interpolation ‘cloud’ for point \mathbf{x} and α_i denote the weighting coefficients. In global interpolation methods, the value of N is equal to the total number of discrete points in the domain. Global methods, while highly accurate, produce interpolation matrices that can have large condition numbers even for modest values of N . Therefore, they are not convenient to solve problems with large numbers of scattered points. The shape parameter influences the accuracy of the interpolation and the condition number of the matrix to evaluate the interpolation coefficients. The prescription of the optimum value of these shape parameters has been one of the difficult issues in the robust use of RBFs for interpolation [55, 56].

Interpolation within a finite number of points in a cloud produces a sparse assembled matrix with a manageable condition number. However, the condition number can still become large for large cloud sizes and large total number of points. Further, with multiquadric, inverse multiquadric and Gaussian interpolations [57] a ‘saturation problem’ can occur, which prevents the discretization errors to asymptotically converge to machine precision. Interpolation with polyharmonic splines does not need the additional shape parameter but also encounters the saturation problem. However, if the PHS-RBF is appended with polynomials [49, 58], the discretization error can be made to decrease exponentially as the degree of the appended polynomial. Also, interpolation using PHS with an appended polynomial converges the discretization errors to machine precision, although appending a polynomial increases the cloud size and the computational work. The coefficients of the PHS-RBF interpolation and of the appended monomials are evaluated by collocating the variable at the scattered locations supplemented with constraints on the appended monomials. The high order of accuracy and convergence to machine precision makes the PHS-RBF interpolation with an appended polynomial an attractive meshless method [59].

In this paper, we describe a multilevel procedure to efficiently solve the Poisson equation in complex domains discretized by the PHS-RBF method. The Poisson equation is encountered while solving numerous engineering problems such as heat conduction, incompressible flows, electromagnetics, porous media flows, etc. Many problems involve irregular solution domains whose accurate discretization and efficient solution are of much importance. Complex domains have been traditionally discretized using curvilinear [62,

63] or unstructured [64, 65] finite difference or finite volume methods. For spectral accuracy, the finite element method has also been combined with Chebyshev polynomial expansions, giving rise to the well-known spectral element method [66–68]. The spectral element method has high accuracy but requires the placement of the points within an element at the specified roots of the polynomials. While the discretization convergence of the finite difference method depends on the order of truncation of the Taylor series, the accuracy of the finite volume method depends on the evaluation of the interface fluxes.

The PHS-RBF discretization can also be formulated to control the local accuracy by selectively varying the degree of the appended polynomial and the spacing between points. This is akin to $(h - p)$ refinement used in higher order finite element and spectral element methods. Discretization of the Poisson equation using the PHS-RBF interpolants over finite sized clouds of points results in a sparse set of linear equations with sparsity proportional to the highest degree of the appended monomial. The condition number of the coefficient matrix usually becomes large, requiring powerful iterative solvers for fast convergence. Conventional single level solvers (such as Jacobi, and SOR) have slow convergence for the long wavelength errors and converge slowly. This motivates us to investigate convergence of multilevel methods as accelerators with low-cost solvers .

The meshless method does not have any underlying grid, and hence is not amenable to traditional nested coarsening or agglomeration of cells. Black-box multigrid procedures based on AMG use heuristic techniques to generate the coarse set of equations. However, this approach has not yet been explored

for meshless methods. Non-nested multilevel procedures in which multiple coarse levels of points are generated either independently or by grouping a few surrounding points into a “mean” point show promise to interpolate variables, residuals, and corrections across levels. To our knowledge, such multilevel methods have not been explored for the PHS- RBF solution of elliptic equations in complex domains. For such non-nested multigrid methods, the interpolation across the various coarse and fine levels of points can be performed using the same radial basis functions also used on the finest set of points. In this work, we describe such a meshless multilevel method for solving the Poisson equation and evaluate its convergence in number of model problems with Dirichlet and all-Neumann boundary conditions. The performance of the method is evaluated for an oscillatory manufactured solution of varying wave number. For all-Neumann boundary conditions the equations are regularized by adding a constraint that makes the linear system well-conditioned [69].

2. The PHS–RBF Method

The PHS-RBF interpolates a function $f(\mathbf{x})$ whose values are known at scattered points using weighted kernels as:

$$f(\mathbf{x}) = \sum_{i=1}^N \alpha_i \phi(\|\mathbf{x} - \mathbf{x}_i\|_2) \quad (3)$$

where ϕ is the polyharmonic spline function given as:

$$\phi(\|\mathbf{x} - \mathbf{x}_i\|_2) = \|\mathbf{x} - \mathbf{x}_i\|_2^{2p+1} \quad (4)$$

and $p = 1, 2, 3$, etc. Further, as mentioned earlier, PHS are appended with number of monomials, the number given by $\binom{l}{d}$, where l is the desired highest degree of the monomial and d is the dimension of the problem. Thus, eq. (3) is extended as:

$$f(\mathbf{x}) = \sum_{i=1}^N \alpha_i \phi(\|\mathbf{x} - \mathbf{x}_i\|_2) + \sum_{j=1}^M \gamma_j P_j(\mathbf{x}) \quad (5)$$

The RBF $\phi(\|\mathbf{x} - \mathbf{x}_i\|_2)$ is a scalar function of the Euclidian distance between the points irrespective of the problem dimension. $P_j(\mathbf{x})$ denotes the j^{th} degree monomial which is weighted by the coefficient γ_j . The $(N + M)$ unknown coefficients are evaluated by collocating the variables at the discrete points and satisfying the constraints on the coefficients of polynomials.

$$\sum_{i=1}^N \alpha_i P_j(\mathbf{x}_i) = 0; \quad j = 1, 2, \dots, M \quad (6)$$

Usually, the total number of cloud points N is selected to be a multiple (around twice) of the number of monomials. The collocation equations and constraints for $\boldsymbol{\alpha}$ and $\boldsymbol{\gamma}$ can be written as:

$$\begin{bmatrix} \boldsymbol{\Phi} & \mathbf{P} \\ \mathbf{P}^T & \mathbf{0} \end{bmatrix} \begin{bmatrix} \boldsymbol{\alpha} \\ \boldsymbol{\gamma} \end{bmatrix} = \begin{bmatrix} \mathbf{f} \\ \mathbf{0} \end{bmatrix} \quad (7)$$

or,

$$[\mathbf{D}] \begin{bmatrix} \boldsymbol{\alpha} \\ \boldsymbol{\gamma} \end{bmatrix} = \begin{bmatrix} \mathbf{f} \\ \mathbf{0} \end{bmatrix} \quad (8)$$

where the superscript T denotes the transpose, $\boldsymbol{\alpha} = [\alpha_1, \dots, \alpha_N]^T$, $\boldsymbol{\gamma} =$

$[\gamma_1, \dots, \gamma_M]^T$, $\mathbf{f} = [f(\mathbf{x}_1), \dots, f(\mathbf{x}_N)]^T$ and $\mathbf{0}$ is the matrix of all zeros of appropriate size. Sizes of the submatrices Φ and \mathbf{P} are $N \times N$ and $N \times M$ respectively. The matrix Φ is given by,

$$\Phi = \begin{bmatrix} \phi(\|\mathbf{x}_1 - \mathbf{x}_1\|_2) & \dots & \phi(\|\mathbf{x}_1 - \mathbf{x}_q\|_2) \\ \vdots & \ddots & \vdots \\ \phi(\|\mathbf{x}_q - \mathbf{x}_1\|_2) & \dots & \phi(\|\mathbf{x}_q - \mathbf{x}_q\|_2) \end{bmatrix} \quad (9)$$

For a polynomial of maximum degree two, the matrix is given as:

$$\mathbf{P} = \begin{bmatrix} 1 & x_1 & y_1 & x_1^2 & x_1 y_1 & y_1^2 \\ \vdots & \vdots & \vdots & \vdots & \vdots & \vdots \\ 1 & x_q & y_q & x_q^2 & x_q y_q & y_q^2 \end{bmatrix} \quad (10)$$

Given the values of \mathbf{f} at the scattered points, the values of α and γ can be evaluated by solving eq. (8). The function \mathbf{f} can then be evaluated at any arbitrary location \mathbf{x} within the cloud. These relations can be implicitly used to determine the discrete values of \mathbf{f} that satisfy a given governing equation at the discrete locations.

To determine the unknown values of the variable, the governing differential equation is collocated at the scattered locations [41, 42]. The derivatives at any location are evaluated by differentiating the analytical interpolation functions and satisfying the governing partial differential equation at every discrete point, thus giving the desired number of equations to determine the values of \mathbf{f} . Let \mathcal{L} denote the Laplacian (∇^2) operator. Then, we can write:

$$\mathcal{L}[f(\mathbf{x})] = \begin{bmatrix} \mathcal{L}[\Phi] & \mathcal{L}[\mathbf{P}] \end{bmatrix} \begin{bmatrix} \alpha \\ \gamma \end{bmatrix} \quad (11)$$

$$= \begin{bmatrix} \mathcal{L}[\Phi] & \mathcal{L}[\mathbf{P}] \end{bmatrix} \begin{bmatrix} \mathbf{D} \end{bmatrix}^{-1} \begin{bmatrix} \mathbf{f} \\ \mathbf{0} \end{bmatrix} = \begin{bmatrix} \mathbf{B}_1 & \mathbf{B}_2 \end{bmatrix} \begin{bmatrix} \mathbf{f} \\ \mathbf{0} \end{bmatrix} = \begin{bmatrix} \mathbf{B}_1 \end{bmatrix} \begin{bmatrix} \mathbf{f} \end{bmatrix} \quad (12)$$

The discrete coefficients for estimation of the Laplacian operator at each point are then combined in a global matrix of n rows (where n is the total number of scattered points), resulting in a set of linear equations given by,

$$\begin{bmatrix} \mathbf{A} \end{bmatrix} \begin{bmatrix} \mathbf{X} \end{bmatrix} = \begin{bmatrix} \mathbf{b} \end{bmatrix} \quad (13)$$

where \mathbf{A} is a sparse matrix of the coefficients of size equal to the number of the scattered points and \mathbf{b} is the vector of the source terms. \mathbf{X} is the vector of all the unknown discrete values. The matrix \mathbf{A} depends only on the coordinates of the cloud points and can be computed and stored at the beginning of the computational algorithm. The computation of the \mathbf{A} matrix requires solution of dense linear systems corresponding to the cloud of each discrete point. However, since the computations for an individual point are independent of others, the coefficients can be computed in parallel. Further economies can be gained by considering groups of points as one cluster and using the same \mathbf{D} matrix for points in the cluster [70].

Any traditional iterative scheme can be used to solve eq. (13). However, the coefficients in \mathbf{A} are highly oscillatory, making traditional solvers slow as well as difficult to converge. Further, single grid iterative solvers are inefficient when the matrix size is large. We describe below a multilevel procedure utilizing non-nested coarsening and appropriate restriction and prolongation procedures.

3. Details of the Multilevel Solution Procedure

Multilevel iterative procedures primarily consist of four main components. First, it is necessary to define coarse levels for solution of the equations for corrections. In hierarchical refinement of structured grids, the fine and coarse grids are nested, and the fine grids are defined by sequentially halving the inter-point distances or subdividing the elements in case of finite element or finite volume methods. Alternatively, the coarse grids can also be defined by progressively agglomerating the finite volumes defined on the finest grid. We use here the concept of non-nested multilevel methods where the individual grids of desired fineness are generated independently. In the context of meshless methods, we use multiple non-nested sets consisting of different numbers of scattered points. The second component of multilevel schemes is the relaxation operator (iterative scheme) used to solve the appropriate discrete equations on any given level. Such a relaxation scheme can range from a point solver (Jacobi, Gauss-Seidel, SOR), to more powerful Krylov sub-space based solvers such as conjugate gradient, BiCGSTAB and GMRES [71]. The third component of multilevel methods is the interpolation procedure to transfer residuals (restriction) from finer levels to coarser level and corrections (prolongation) from coarser level to finer level. In geometry-based multilevel methods, restriction and prolongation operators are constructed by distance weighting using bilinear or trilinear interpolation. In non-nested multigrid methods, the restriction and prolongation require interpolation across scattered points. Finally, a cycling strategy that defines the sequence in which the fine and coarse levels are visited needs to be specified. On any level the number of relaxations can be fixed or adaptively

controlled based on the convergence rate. Details of these four steps in our algorithm are given below.

3.1. Generation of Coarse Level Point Sets

As mentioned earlier, the meshless discretization only uses scattered points with no explicit connectivity. The points can be generated by many procedures of choice, including by conventional finite element mesh generation techniques. A straight-forward way to generate scattered points is to use an established finite element mesh generator and extract only the coordinates of the vertices. In meshless techniques, because of the absence of connectivity between the points, quality of the grid as characterized by the slenderness of the elements does not explicitly affect accuracy of discretization. However, the inter-point spacings and the total number of points influence the condition number and solvability of the system of equations. In the present study, we generated the point sets on multiple levels using an open-source finite element grid generator, Gmsh [72].

3.2. Relaxation Operator

The coefficient matrix \mathbf{A} in eq. (13) is computed and stored in sparse row column (CSR) format consistent with the Eigen library [73]. At Dirichlet boundaries, where the values are known, the interior equations are condensed with substitution of the boundary values. For Neumann boundaries, special clouds for the boundary points are defined which contain only interior points and no points on the boundary. The discrete equations of the boundary points are then substituted into the equations of the interior points, resulting in an implicit coupling of the boundary and interior points. The matrix

of coefficients is then re-ordered using the Reverse Cuthill-McGee (RCM) [74] algorithm to reduce bandwidth and increase computational efficiency. Currently we use the SOR point solver with an over-relaxation factor of 1.4 as the relaxation scheme. The SOR is the most efficient of the point solvers, although the Jacobi solver is better suited for parallelization. Other solvers such as ILU with drop tolerance, preconditioned BiCGSTAB and GMRES can also be used along with the multilevel method. In Section 4.4 we evaluate a combination of GMRES and the multilevel algorithm.

3.3. Restriction and Prolongation Operators

For the linear Poisson equation, a correction multilevel scheme is appropriate. Only the residuals need to be restricted from a fine level to a coarser level. The residuals on the finer level are calculated after a prescribed number of relaxations as:

$$\mathbf{R}^h = \mathbf{b}^h - \mathbf{A}^h \mathbf{X}^h \quad (14)$$

where the superscript h refers to the set of points on the finer level and \mathbf{R} , \mathbf{b} , and \mathbf{X} are vectors that denote the residual, the right-hand side, and the solution respectively. The residuals at the coarser set of points, denoted with superscript H are obtained by applying the interpolation operator \mathbf{I}_h^H which restricts the residuals as:

$$\mathbf{R}^H = \mathbf{I}_h^H \mathbf{R}^h \quad (15)$$

The interpolation operator \mathbf{I}_h^H is constructed as follows. Given the coordinates of the coarse and fine sets of points, we first identify a cloud of closest fine level points for each one of the coarse set points. The number of

fine level points for each coarse set point depends on the desired accuracy of the interpolation. We use the same PHS-RBF interpolation procedure with appended polynomial as described earlier and a graphical representation of this interpolation operation is given in fig. 1.

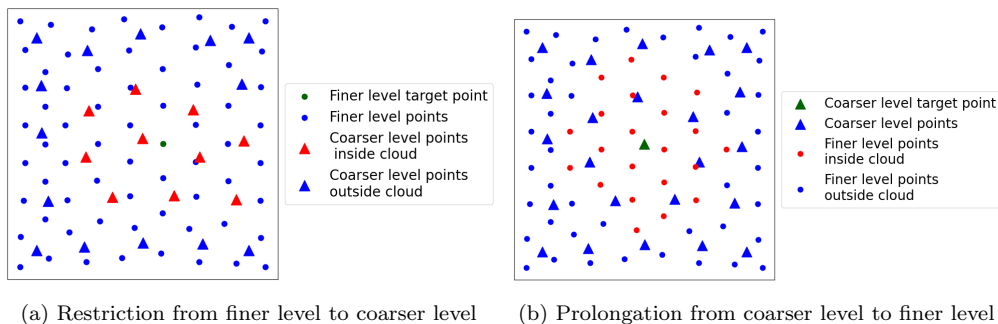


Figure 1: PHS-RBF interpolation between finer and coarser levels on a square geometry

The order of accuracy for restricting residuals can be the same as the order of accuracy used for discretization of the partial derivatives in the governing equation or it can be lower. To construct the restriction interpolation matrices, we start with the interpolation of fine level points over the selected cloud, as:

$$f(\mathbf{x}^h) = \sum_{i=1}^{N^h} \alpha_i \phi(\|\mathbf{x}^h - \mathbf{x}_i^h\|_2) + \sum_{j=1}^{M^h} \gamma_j P_j(\mathbf{x}^h) \quad (16)$$

where N^h spans the cloud of fine points for a given coarse level point, and M^h represents the number of appended monomials. Collocation of the fine set values at the discrete points of interpolation gives the coefficients α and γ . The function value is then evaluated at the coordinates of the coarse point. The resulting weights multiplying the fine set values to the coarse set points are evaluated at the beginning of the solution procedure and stored

in a sparse rectangular matrix. Such matrices are computed for every pair of fine and coarse levels. We observed that the order of accuracy of interpolations need not be as high as the discretization accuracy used on the finest level as it did not noticeably affect the rate of the multilevel convergence. Using a lower order polynomial in the PHS-RBF interpolation matrix however saves some CPU time. At the boundary points, the residuals are implicitly zero because the boundary equations are substituted in the interior equations. The boundary equations are therefore not solved explicitly. After the boundary equations are eliminated, the equations for the interior points are reordered using the RCM ordering.

When the down-leg is completed, the corrections are successively prolonged to the points on the finer levels. For prolongation, we again compute the interpolation matrices by first defining the cloud of coarse set points to be used in the interpolation for each point on a finer level. The prolongation matrices are computed in the same way as the restriction matrices by first determining the PHS-RBF coefficients in the coarse point interpolation and then determining the weights of each coarse point for a given fine level point. Thus, each fine level value is corrected as:

$$\mathbf{X}^h = \mathbf{X}^h + \mathbf{I}_H^h \delta \mathbf{X}^H \quad (17)$$

For Dirichlet boundary conditions, the corrections on the boundaries are zero. However, for Neumann conditions, the corrections at the boundary points are evaluated from the interior coarse grid corrections using the discretized Neumann condition which was earlier substituted into the interior equations. Prolongations are also followed by a relaxation step. Both the

restriction and prolongation matrices are calculated upfront of the iterations. Note that the current restriction and prolongation operators are based solely on the geometric coordinates of the points and do not take into account the strengths of the coefficients, as in AMG.

4. Results

4.1. Problems Considered

The performance of the above algorithm is evaluated for the solution of the Poisson equation in three model geometries using a manufactured solution. A manufactured solution satisfies a governing equation with appropriate additional source terms obtained by substituting the manufactured solution in the governing equation. We consider the manufactured solution:

$$T(x, y) = \cos(k\pi x) \cos(k\pi y) \quad (18)$$

which satisfies the Poisson equation,

$$\nabla^2 T(x, y) = -2\pi^2 k^2 \cos(k\pi x) \cos(k\pi y) \quad (19)$$

where k is the wavenumber of the manufactured solution. To test the robustness of the multilevel convergence, we varied a) geometry; b) wavenumber; c) type of boundary condition (Dirichlet and Neumann); d) number of scattered points on the finest level; e) number of levels in the multilevel cycling and f) the degree of the highest appended monomial in the PHS-RBF discretization. For Dirichlet conditions, the exact analytical values are prescribed on the boundaries, while the exact analytical derivatives are pre-

scribed for the Neumann boundary condition. The effect of the order of the polynomial for constructing coarse level restriction / prolongation and discretization operators on the multilevel performance was also investigated. We found that using a lower order polynomial for interpolation and discretization on the coarser levels did not noticeably affect the multilevel performance but provided a slightly reduced computational work. The use of lower order polynomial on the coarse levels does not influence the accuracy of the final solution obtained on the finest level.

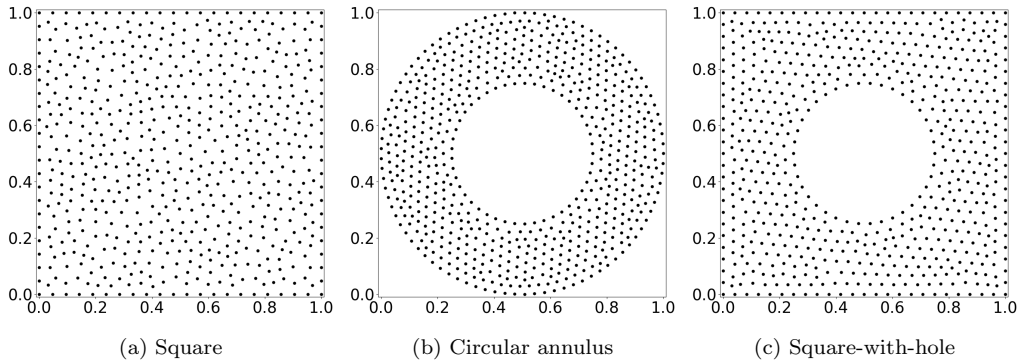


Figure 2: Geometries considered and layout of discrete points

Figure 2 shows the three geometries considered in this study. The scattered points shown were obtained from vertices of triangles generated by an open-source mesh generation software [72]. For each geometry, sets with different numbers of scattered points were obtained using the same software.

Geometry/Level	Square	Concentric annulus	Square-with-hole
1	98	90	89
2	169	188	176
3	607	650	640
4	2535	2581	2532
5	10023	10207	10197

Table 1: Numbers of points for each problem on different levels

Table 1 gives the numbers of points used for each problem on different levels. The discretization accuracy was computed as the L_1 norm of the difference between the converged discrete solution and the analytical solution defined as:

$$E = \frac{\sum_{i=1}^n |T_{PHS} - T_{exact}|_i}{\sum_{i=1}^n |T_{exact}|_i} \quad (20)$$

Convergence of the equations was monitored by the L_1 norm of the residuals defined as:

$$E = \frac{\sum_{i=1}^n |\nabla^2 T_{PHS} - RHS|_i}{\sum_{i=1}^n |RHS|_i} \quad (21)$$

The multilevel iterations were continued until the residual norm reached a value below 10^{-10} . The initial values for the variables were always set to zero, and the residuals were normalized with the norm of the source terms. At any iteration, the residuals were evaluated at the top of the V-cycle. At each level, the residuals were relaxed with five SOR iterations after which they were restricted to the next coarser level. Five SOR relaxations were

also performed after prolongating the corrections to a finer level. An over-relaxation parameter of 1.4 was used on all levels.

4.2. Results for Dirichlet Boundary Conditions

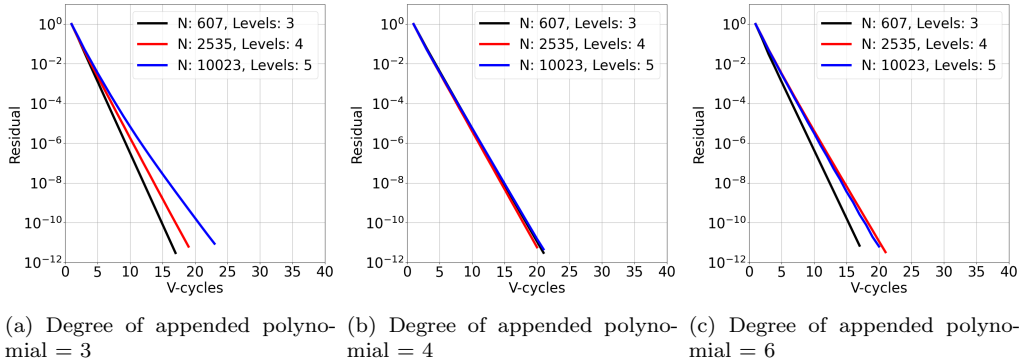


Figure 3: Convergence of the residual on a square with Dirichlet boundary conditions

Systematic calculations were performed for each geometry by varying the highest degree of the appended monomials, number of scattered points on the finest level, and the wavenumber of the manufactured solution. The highest degree of the appended monomials was varied between 3 and 6, and five levels of points were considered with the largest set consisting around 10,000 points. The wavenumber was varied between 1 and 4. Figure 3 shows selected multilevel convergence histories for the square geometry using wavenumber $k = 1$ and three sets of points with polynomial degree of 3, 4, and 6. For each calculation, the coarsest level had 98 points. The number of points on all levels are given in table 1. It is seen that the residual is quickly reduced by about ten orders of magnitude in less than 20 V-cycles, although the multilevel convergence is not exactly uniform with point density. The polynomial degree for restriction/prolongation and discretization on the

coarse levels is kept at three. Increasing this did not improve the convergence shown in fig. 3. Alternative cycles such as the W-cycle and adaptive V-cycle may improve convergence but have not been explored in current study.

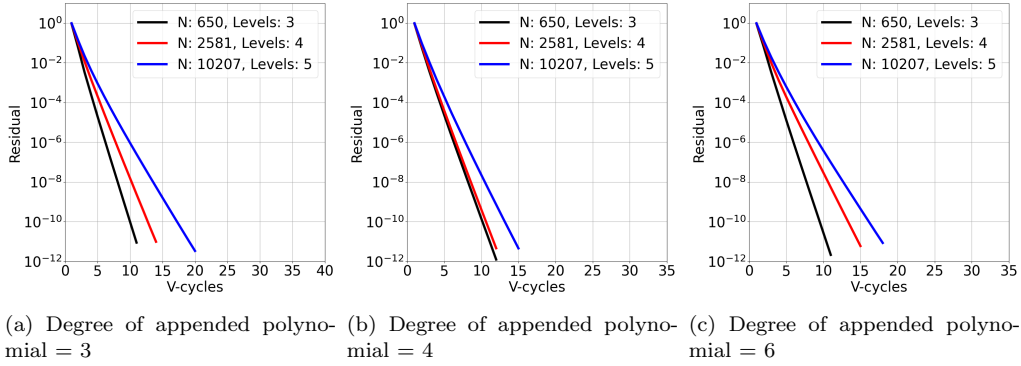


Figure 4: Convergence of the residual on a concentric annulus with Dirichlet boundary conditions

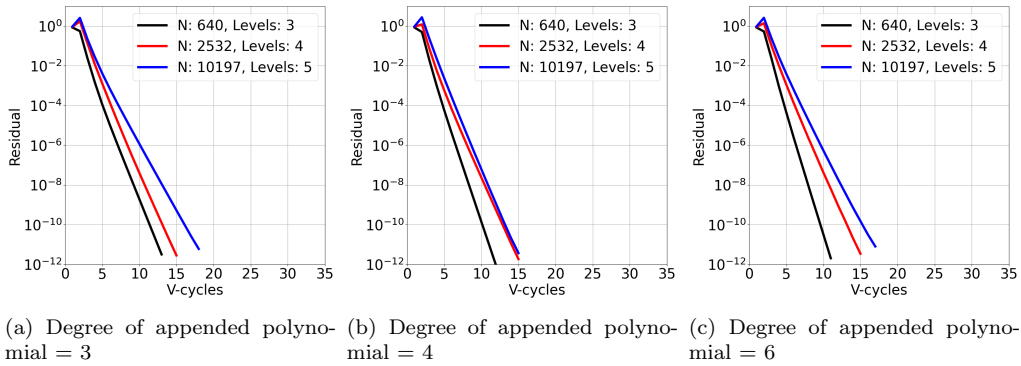


Figure 5: Convergence of the residual on a square-with-hole geometry with Dirichlet boundary conditions

Figures 4 and 5 show similar convergence histories for the concentric annulus and the square-with-hole geometries respectively. The rates of convergence for these problems are also fast as convergence is achieved in typically 10 to 20 V-cycles for ten orders of residual reduction. However, convergence

for larger point sets required more V cycles than for smaller sets, displaying some multigrid inefficiency. The coefficients in the meshless discretization are oscillatory, and the SOR with 5 relaxation sweeps is probably not sufficient to efficiently annihilate the high frequency errors and may require more relaxation sweeps.

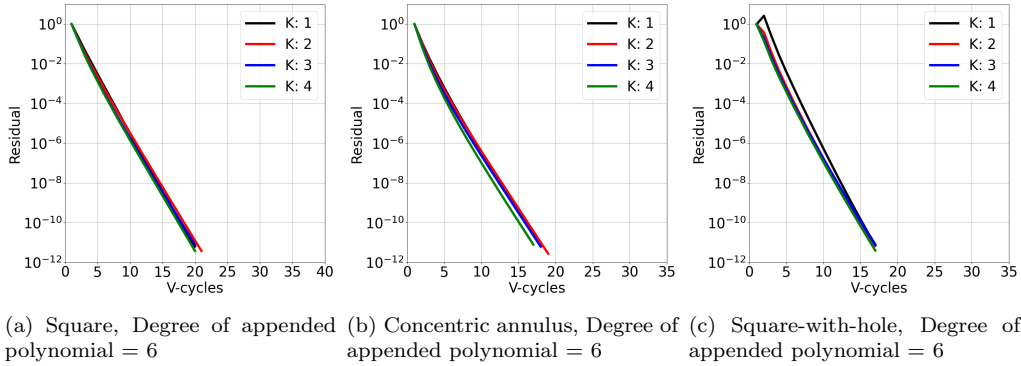


Figure 6: Effect of the wavenumber of the manufactured solution on multilevel convergence for finest level

Figure 6 shows the rates of convergence for different wavenumbers of the manufactured solution. Higher wavenumbers have more oscillatory behavior and therefore can converge faster. The results presented correspond to a point set consisting of around $\sim 10,000$ points with an appended polynomial of degree 6. The coarsest set has ~ 90 points (5 levels). We observe that all wavenumbers converge at nearly the same rate. Thus, henceforth, the calculations are performed by fixing the wavenumber k at 1.

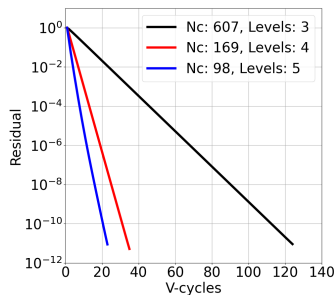


Figure 7: Effect of coarsest level on multilevel convergence

Figure 7 shows the rates of convergence for the square geometry with different degrees of coarsening. The finest level (5) was kept the same with 10,023 points and the appended polynomial degree was fixed at $l=3$. The coarsest level was varied from 1 (98 points) to 3 (607 points). It is seen that a factor of 5 reduction in the number of V cycles is obtained by cycling up to level 1 versus cycling only to the third level. This factor was slightly different for other problems, and for other degrees of appended polynomials. As expected, convergence was better with the coarsest level having 98 points. The number of iterations with only a single level relaxation was significantly greater and not included here.

4.3. Results for All Neumann Boundary Conditions

We next present results for Neumann conditions prescribed on all the boundaries. The analytical derivative given by the manufactured solution was imposed at all the points on the boundaries. Note that when all the boundaries are of Neumann type, the problem is ill-conditioned as the solution can only be computed to an arbitrary constant. Hence the matrix must be regularized either by fixing one of the points to some arbitrary value or imposing a global constraint on the values. Here we use the regularization

procedure in which the sum of all values was assigned an arbitrary level of zero [69]. The solution matrix was therefore modified by adding an extra equation of unity coefficients and zero right-hand side. Figures 8 to 10 show the multilevel convergence for the three problems with all Neumann boundary conditions. SOR with over-relaxation factor of 1.4 was used with five (5) iterations. It is seen that even after regularization, the convergence rate is not satisfactory. Compared with the case of Dirichlet boundary condition, the Neumann condition took more V-cycles to converge, and the convergence depended on the refinement. Some of the computations even diverged, especially for high degree of polynomial ($l = 6$). In the case of square-with-hole geometry, limiting the coarsest level to 176 points gave better convergence.

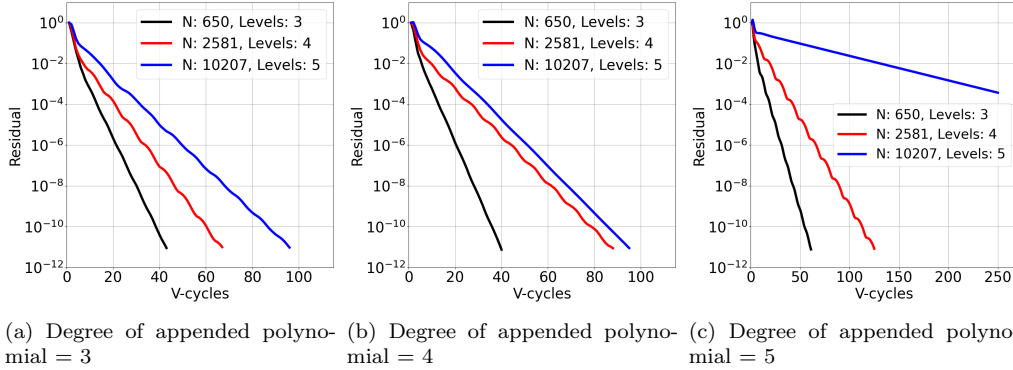


Figure 8: Convergence of the residual on a concentric annulus with all-Neumann boundary conditions

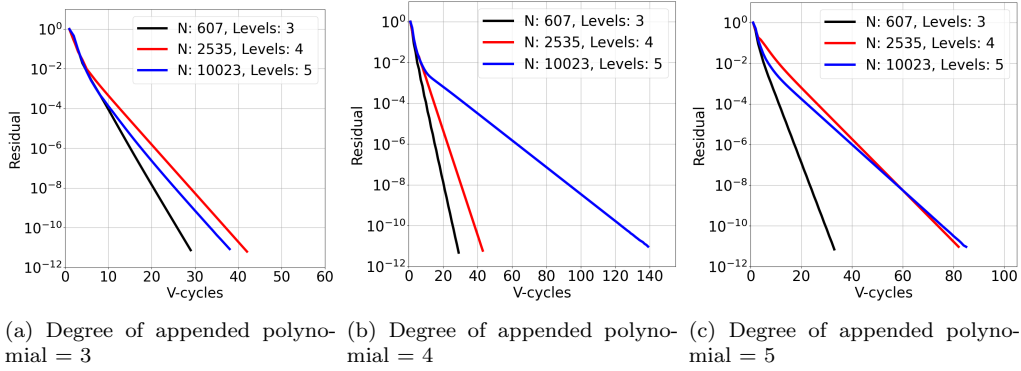


Figure 9: Convergence of the residual on a square geometry with all-Neumann boundary conditions

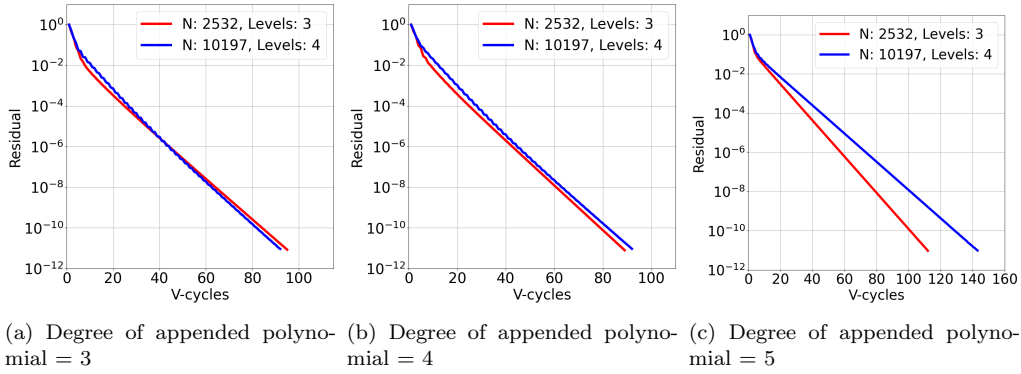


Figure 10: Convergence of the residual on a square-with-hole geometry with all-Neumann boundary conditions (coarsest level = 176 points)

4.4. Multilevel Preconditioned GMRES

The all-Neumann boundary condition is important in many fields including for determination of the pressure field in simulations of incompressible fluid flows with prescribed boundary conditions. Since the multilevel solver with pure SOR relaxation converged slowly for cases of the all-Neumann boundary conditions, we explored a combination of GMRES and the multilevel algorithm in which the multilevel algorithm is used to resolve the

residuals computed inside a Krylov Subspace Projector (KSP). Five sweeps of the SOR are also performed at each level, but residuals to be smoothed are calculated by the GMRES algorithm on the finest level. The pseudo code for this algorithm is given below:

Pseudocode for Multilevel Preconditioned GMRES Algorithm

Let $x = 0$, $r = b$, $k = 0$, $\text{tol} = 10^{-10}$

while(true)

$k++$

 Solve $M_g z = r$

 if($k == 1$)

$p_k = z$

$w_k = Ap_k$

 else

$p_k = z$

 for $i = 1 \dots k - 1$

$p_k = p_k - [(w_i)^T(Az)/(w_i)^T(w_i)]$

$w_k = Ap_k$

$\alpha = (w_k)^T(Ar)/(w_k)^T(w_k)$

$x = x + \alpha p_k$

$r = r - \alpha w_k$

 if (($\|r\|/\|b\|$) < tol)

 break

Here, p_k 's are mutually orthogonal in the $A^T A$ norm, which is Symmetric

Positive Definite (SPD) even if A is not SPD. Thus, the updated solution is the best fit in the space of the p_k 's in the $A^T A$ norm. Note that we have used modified Gram-Schmidt procedure to orthogonalize the search directions for better numerical stability. The solution to $M_g z = r$ applies one V-cycle of the multilevel operator M_g with the righthand side vector as r . The multilevel procedure starts with an initial vector of zero corrections and stores the result after one V-cycle in the vector z . This procedure was seen to be efficient and robust for all the pure Neumann boundary condition cases. Also, the number of V-cycles was not observed to increase very much with polynomial degree, although the condition number increases significantly with the degree of the appended polynomial.

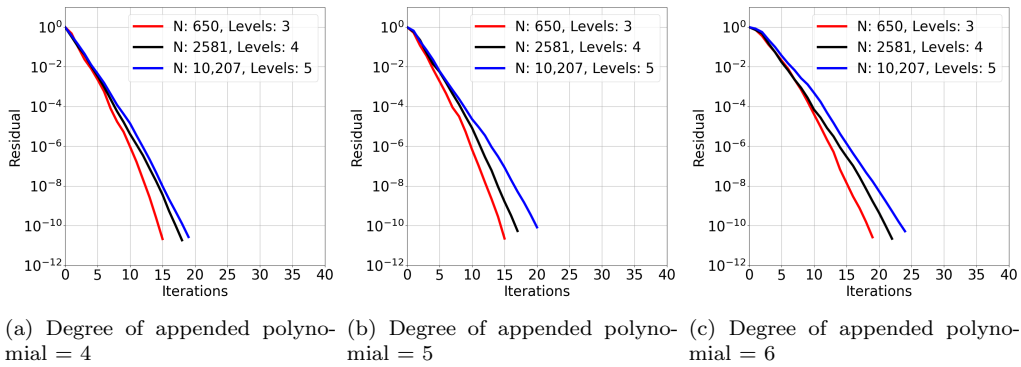


Figure 11: Convergence of the GMRES-Multilevel algorithm for the concentric annulus with all-Neumann boundary conditions

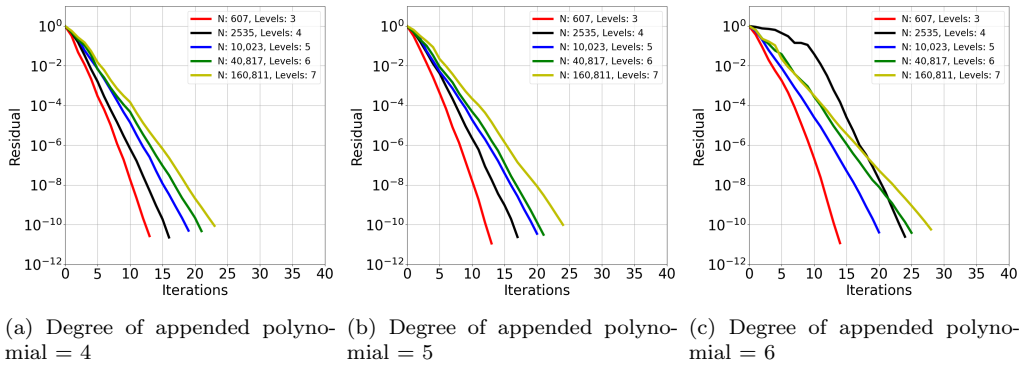


Figure 12: Convergence of the GMRES-Multilevel algorithm for the square geometry with all-Neumann boundary conditions

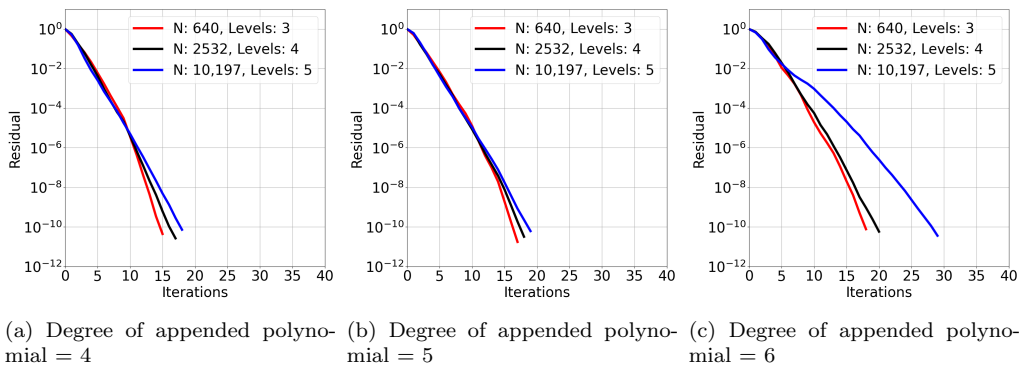


Figure 13: Convergence of the GMRES-Multilevel algorithm for the square-with-hole geometry with all-Neumann boundary conditions

Figures 11 to 13 show convergence histories of this algorithm for the wavenumber $k = 1$ and for the three geometries. It is seen that the combination of GMRES with the multilevel solver for the residuals gives fast convergence for the all-Neumann boundary condition. Although all point sets do not converge at same rates, the multilevel property is nearly achieved. The slightly slower convergence for higher order polynomial cases may be a result of the condition number, and the large bandwidth of the sparse coefficient

cient matrix. Other relaxation schemes such a block-SOR may provide faster convergence and will be explored in future studies.

4.5. Discretization Error

As mentioned earlier, the PHS-RBF method displays exponential convergence with point spacing as per the degree of the appended polynomial. The accuracy of the present solutions for the three geometries is demonstrated by plotting below the differences from the known manufactured solutions. For a given degree of the polynomial l , the second derivative displays at least $(l-1)$ degree of accuracy.

The calculated errors for each case are plotted in fig. 14 for polynomial degree of 5 against an average spacing Δx defined as:

$$\Delta x = (Ar/n)^{0.5} \tag{22}$$

where Ar and n in eq. (22) refer to the area of the domain and number of points respectively.

The errors are seen to follow the expected trends. It must be pointed out that both the point spacings and polynomial order can be also varied locally as well as globally. This gives more freedom in targeting accuracy to desired regions through combined refinements in point spacing as well as the polynomial degree.

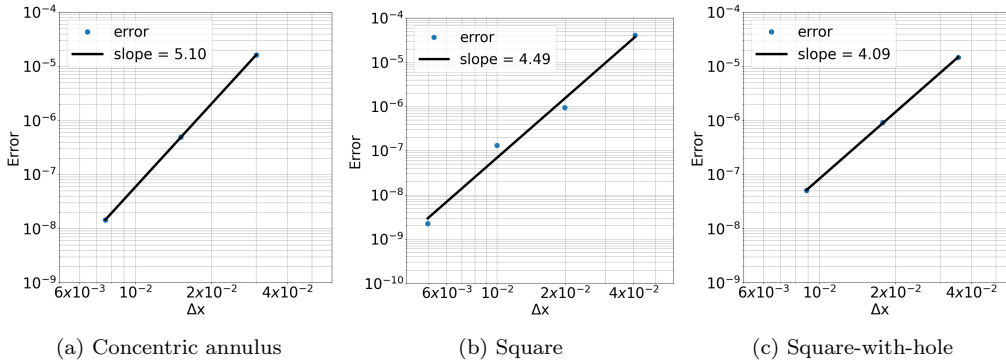


Figure 14: Discretization errors for the three geometries with degree of appended polynomial of 5.

5. Summary and Future Research

We have presented in this paper a multilevel algorithm for solving the discrete equations resulting from meshless discretization of the Poisson equation in a complex domain. The meshless discretization is done by scattered data interpolation using polyharmonic splines with appended polynomials of high degree. The multilevel algorithm uses non-nested point sets and restriction/prolongations using the PHS-RBF interpolations. Systematic tests have been performed for three different geometries using manufactured solutions. The algorithm is seen to converge rapidly for Dirichlet boundary conditions for large number of scattered points and for high order appended polynomials. However, for the case of all-Neumann boundary condition, the convergence with pure SOR is seen to be inferior and not be robust. The multilevel method was then investigated as a preconditioner to a GMRES algorithm. Good and robust convergence has been achieved for the all-Neumann cases. The Multilevel preconditioned GMRES algorithm is then implemented in a fractional step algorithm to solve the pressure Poisson equation. Good con-

vergence is seen for two model problems tested with approximately 10,000 scattered points (Kovasznay flow [75] and flow between two concentric cylinders due to a rotating inner cylinder). Future efforts will be directed towards extensions to three-dimensions and parallelization of the entire algorithm including the coefficient computations. Implementation on massively parallel architectures such as the GPU will also be pursued.

References

- [1] A. Brandt, Multi-level adaptive solutions to boundary-value problems, *Mathematics of Computation* 31 (138) (1977) 333–390.
- [2] U. Trottenberg, C. W. Oosterlee, A. Schuller, *Multigrid*, Elsevier, 2000.
- [3] W. L. Briggs, V. E. Henson, S. F. McCormick, *A multigrid tutorial*, SIAM, 2000.
- [4] I. Yavneh, Why multigrid methods are so efficient, *Computing in Science & Engineering* 8 (6) (2006) 12–22.
- [5] K. Stüben, U. Trottenberg, Multigrid methods: Fundamental algorithms, model problem analysis and applications, *Multigrid Methods* (1982) 1–176.
- [6] L. Bairstow, A. Berry, Two-dimensional solutions of Poisson’s and Laplace’s equations, *Proceedings of the Royal Society of London. Series A, Containing Papers of a Mathematical and Physical Character* 95 (672) (1919) 457–475.

- [7] H. Bateman, A partial differential equation associated with Poisson's work on the theory of sound, *American Journal of Mathematics* 60 (2) (1938) 293–296.
- [8] M. Shimada, H. Tokunaga, N. Satofuka, H. Nishida, Numerical simulation of three-dimensional viscous flows using the vector potential method, *JSME international journal. Ser. 2, Fluids engineering, heat transfer, power, combustion, thermophysical properties* 34 (2) (1991) 109–114.
- [9] F. H. Harlow, J. E. Welch, Numerical calculation of time-dependent viscous incompressible flow of fluid with free surface, *Physics of Fluids* 8 (12) (1965) 2182–2189.
- [10] G. Pöplau, U. Van Rienen, Multigrid solvers for Poisson's equation in computational electromagnetics, in: *Scientific Computing in Electrical Engineering*, Springer, 2001, pp. 169–176.
- [11] B. Koobus, M.-H. Lallemand, A. Dervieux, Unstructured volume-agglomeration mg: Solution of the Poisson equation, *International Journal for Numerical Methods in Fluids* 18 (1) (1994) 27–42.
- [12] T. F. Chan, J. Xu, L. Zikatanov, An agglomeration multigrid method for unstructured grids, *Contemporary Mathematics* 218 (1998) 67–81.
- [13] V. Venkatakrishnan, D. J. Mavriplis, Agglomeration multigrid for the three-dimensional Euler equations, *AIAA journal* 33 (4) (1995) 633–640.
- [14] M.-H. Lallemand, H. Steve, A. Dervieux, Unstructured multigriding

- by volume agglomeration: Current status, *Computers & Fluids* 21 (3) (1992) 397–433.
- [15] F. Bassi, L. Botti, A. Colombo, D. A. Di Pietro, P. Tesini, On the flexibility of agglomeration based physical space discontinuous galerkin discretizations, *Journal of Computational Physics* 231 (1) (2012) 45–65.
- [16] S. Langer, Agglomeration multigrid methods with implicit runge–kutta smoothers applied to aerodynamic simulations on unstructured grids, *Journal of Computational Physics* 277 (2014) 72–100.
- [17] D. Mavriplis, V. Venkatakrishnan, A 3D agglomeration multigrid solver for the Reynolds–averaged Navier–Stokes equations on unstructured meshes, *International Journal for Numerical Methods in Fluids* 23 (6) (1996) 527–544.
- [18] G. Carré, An implicit multigrid method by agglomeration applied to turbulent flows, *Computers & Fluids* 26 (3) (1997) 299–320.
- [19] A. Settari, K. Aziz, A generalization of the additive correction methods for the iterative solution of matrix equations, *SIAM Journal on Numerical Analysis* 10 (3) (1973) 506–521.
- [20] B. Hutchinson, P. Galpin, G. Raithby, Application of additive correction multigrid to the coupled fluid flow equations, *Numerical Heat Transfer* 13 (2) (1988) 133–147.
- [21] A. Brandt, Algebraic multigrid theory: The symmetric case, *Applied Mathematics and Computation* 19 (1-4) (1986) 23–56.

- [22] J. W. Ruge, K. Stüben, Algebraic multigrid, in: *Multigrid Methods*, SIAM, 1987, pp. 73–130.
- [23] U. M. Yang, et al., BoomerAMG: A parallel algebraic multigrid solver and preconditioner, *Applied Numerical Mathematics* 41 (1) (2002) 155–177.
- [24] J. Dendy, Black box multigrid, *Journal of Computational Physics* 48 (3) (1982) 366–386.
- [25] M. L. Bittencourt, C. C. Douglas, R. A. Feijóo, Nonnested multigrid methods for linear problems, *Numerical Methods for Partial Differential Equations: An International Journal* 17 (4) (2001) 313–331.
- [26] M. L. Bittencourt, C. C. Douglas, R. A. Feijóo, Adaptive non-nested multigrid methods, *Engineering Computations* 19 (2) (2002) 158–176.
- [27] P. F. Antonietti, G. Pennesi, V-cycle multigrid algorithms for discontinuous Galerkin methods on non-nested polytopic meshes, *Journal of Scientific Computing* 78 (1) (2019) 625–652.
- [28] A. Katz, A. Jameson, Multicloud: Multigrid convergence with a meshless operator, *Journal of Computational Physics* 228 (14) (2009) 5237–5250.
- [29] R. Wienands, C. W. Oosterlee, T. Washio, Fourier analysis of GMRES (m) preconditioned by multigrid, *SIAM Journal on Scientific Computing* 22 (2) (2000) 582–603.

- [30] N. M. Evstigneev, Numerical analysis of Krylov multigrid methods for stationary advection-diffusion equation, in: *Journal of Physics: Conference Series*, Vol. 1391, IOP Publishing, 2019, p. 012080.
- [31] H. C. Elman, O. G. Ernst, D. P. O’Leary, A multigrid method enhanced by Krylov subspace iteration for discrete Helmholtz equations, *SIAM Journal on Scientific Computing* 23 (4) (2001) 1291–1315.
- [32] Y. A. Erlangga, C. W. Oosterlee, C. Vuik, A novel multigrid based preconditioner for heterogeneous Helmholtz problems, *SIAM Journal on Scientific Computing* 27 (4) (2006) 1471–1492.
- [33] J. Xu, The auxiliary space method and optimal multigrid preconditioning techniques for unstructured grids, *Computing* 56 (3) (1996) 215–235.
- [34] S. P. Vanka, Block-implicit multigrid solution of Navier-Stokes equations in primitive variables, *Journal of Computational Physics* 65 (1) (1986) 138–158.
- [35] V. John, L. Tobiska, Numerical performance of smoothers in coupled multigrid methods for the parallel solution of the incompressible Navier–Stokes equations, *International Journal for Numerical Methods in Fluids* 33 (4) (2000) 453–473.
- [36] M. Thompson, J. H. Ferziger, An adaptive multigrid technique for the incompressible Navier-Stokes equations, *Journal of Computational Physics* 82 (1) (1989) 94–121.
- [37] M. Paisley, Multigrid solution of the incompressible Navier–Stokes equations for three-dimensional recirculating flow: Coupled and decoupled

- smoothers compared, *International Journal for Numerical Methods in Fluids* 30 (4) (1999) 441–459.
- [38] S. Sivaloganathan, G. Shaw, A multigrid method for recirculating flows, *International Journal for Numerical Methods in Fluids* 8 (4) (1988) 417–440.
- [39] D. J. Mavriplis, A. Jameson, Multigrid solution of the Navier-Stokes equations on triangular meshes, *AIAA Journal* 28 (8) (1990) 1415–1425.
- [40] R. L. Hardy, Multiquadric equations of topography and other irregular surfaces, *Journal of Geophysical Research* 76 (8) (1971) 1905–1915.
- [41] E. J. Kansa, Multiquadrics—a scattered data approximation scheme with applications to computational fluid-dynamics—i surface approximations and partial derivative estimates, *Computers & Mathematics with Applications* 19 (8-9) (1990) 127–145.
- [42] E. J. Kansa, Multiquadrics—a scattered data approximation scheme with applications to computational fluid-dynamics—ii solutions to parabolic, hyperbolic and elliptic partial differential equations, *Computers & Mathematics with Applications* 19 (8-9) (1990) 147–161.
- [43] C. Franke, R. Schaback, Solving partial differential equations by collocation using radial basis functions, *Applied Mathematics and Computation* 93 (1) (1998) 73–82.
- [44] G. E. Fasshauer, Solving partial differential equations by collocation with radial basis functions, in: *Proceedings of Chamonix, Vol. 1997*, Citeseer, 1996, pp. 1–8.

- [45] C. Shu, H. Ding, K. Yeo, Local radial basis function-based differential quadrature method and its application to solve two-dimensional incompressible Navier–Stokes equations, *Computer Methods in Applied Mechanics and Engineering* 192 (7-8) (2003) 941–954.
- [46] H. Ding, C. Shu, K. Yeo, D. Xu, Numerical simulation of flows around two circular cylinders by mesh-free least square-based finite difference methods, *International Journal for Numerical Methods in Fluids* 53 (2) (2007) 305–332.
- [47] Y. Sanyasiraju, G. Chandhini, Local radial basis function based gridfree scheme for unsteady incompressible viscous flows, *Journal of Computational Physics* 227 (20) (2008) 8922–8948.
- [48] S. Wong, Y. Hon, M. A. Golberg, Compactly supported radial basis functions for shallow water equations, *Applied Mathematics and Computation* 127 (1) (2002) 79–101.
- [49] S. Shahane, A. Radhakrishnan, S. P. Vanka, A high-order accurate meshless method for solution of incompressible fluid flow problems, *arXiv preprint arXiv:2010.01702* (2020).
- [50] C. Franke, R. Schaback, Convergence order estimates of meshless collocation methods using radial basis functions, *Advances in Computational Mathematics* 8 (4) (1998) 381–399.
- [51] D. Yun, Y. Hon, Improved localized radial basis function collocation method for multi-dimensional convection-dominated problems, *Engineering Analysis with Boundary Elements* 67 (2016) 63–80.

- [52] G. C. Bourantas, B. F. Zwick, G. R. Joldes, V. C. Loukopoulos, A. C. Tavner, A. Wittek, K. Miller, An explicit meshless point collocation solver for incompressible Navier-Stokes equations, *Fluids* 4 (3) (2019) 164.
- [53] J. Yang, M. Potier-Ferry, H. Hu, Solving the stationary Navier–Stokes equations by using Taylor meshless method, *Engineering Analysis with Boundary Elements* 98 (2019) 8–16.
- [54] C. Varanasi, J. Y. Murthy, S. Mathur, A meshless finite difference method for conjugate heat conduction problems, *Journal of Heat Transfer* 132 (8) (2010).
- [55] M. D. Buhmann, *Radial basis functions: Theory and implementations*, Vol. 12, Cambridge University Press, 2003.
- [56] R. Franke, G. Nielson, Smooth interpolation of large sets of scattered data, *International Journal for Numerical Methods in Engineering* 15 (11) (1980) 1691–1704.
- [57] B. Fornberg, E. Larsson, N. Flyer, Stable computations with Gaussian radial basis functions, *SIAM Journal on Scientific Computing* 33 (2) (2011) 869–892.
- [58] N. Flyer, B. Fornberg, V. Bayona, G. A. Barnett, On the role of polynomials in RBF-FD approximations: I. interpolation and accuracy, *Journal of Computational Physics* 321 (2016) 21–38.

- [59] V. Bayona, N. Flyer, B. Fornberg, G. A. Barnett, On the role of polynomials in RBF-FD approximations: II. numerical solution of elliptic pdes, *Journal of Computational Physics* 332 (2017) 257–273.
- [60] G. A. Barnett, A robust RBF-FD formulation based on polyharmonic splines and polynomials, Ph.D. thesis, PhD thesis, University of Colorado Boulder (2015).
- [61] D. Miotti, R. Zamolo, E. Nobile, A fully meshless approach to the numerical simulation of heat conduction problems over arbitrary 3D geometries, *Energies* 14 (5) (2021) 1351.
- [62] J. D. Anderson, *Computational Fluid Dynamics: The Basics with Applications*, McGraw-Hill, 1995.
- [63] R. H. Pletcher, J. C. Tannehill, D. Anderson, *Computational Fluid Mechanics and Heat Transfer*, CRC press, 2012.
- [64] C. A. Fletcher, *Computational Techniques for Fluid Dynamics*, Vol. 1, Springer, 1991.
- [65] S. Mathur, J. Murthy, A pressure-based method for unstructured meshes, *Numerical Heat Transfer* 31 (2) (1997) 195–215.
- [66] P. F. Fischer, A. T. Patera, Parallel spectral element methods for the incompressible Navier-Stokes equations, in: *Solution of Superlarge Problems in Computational Mechanics*, Springer, 1989, pp. 49–65.
- [67] H. Xu, C. D. Cantwell, C. Monteserin, C. Eskilsson, A. P. Engsig-Karup, S. J. Sherwin, Spectral/hp element methods: Recent developments, ap-

- lications, and perspectives, *Journal of Hydrodynamics* 30 (1) (2018) 1–22.
- [68] G. Karniadakis, S. Sherwin, *Spectral/hp element methods for computational fluid dynamics*, Oxford University Press, 2013.
- [69] Poisson equation with pure Neumann boundary conditions (2019).
URL <https://fenicsproject.org/olddocs/dolfin/2016.2.0/python/demo/documentated/neumann-poisson/python/documentation.html>
- [70] V. Shankar, The overlapped radial basis function-finite difference (RBF-FD) method: A generalization of RBF-FD, *Journal of Computational Physics* 342 (2017) 211–228.
- [71] Y. Saad, M. H. Schultz, GMRES: A generalized minimal residual algorithm for solving nonsymmetric linear systems, *SIAM Journal on Scientific Computing* 7 (3) (1986) 856–869.
- [72] C. Geuzaine, J.-F. Remacle, Gmsh: A 3D finite element mesh generator with built-in pre-and post-processing facilities, *International Journal for Numerical Methods in Engineering* 79 (11) (2009) 1309–1331.
- [73] G. Guennebaud, B. Jacob, et al., *Eigen v3* (2020).
URL <http://eigen.tuxfamily.org>
- [74] E. Cuthill, J. McKee, Reducing the bandwidth of sparse symmetric matrices, *ACM: Proceedings of the 24th national conference*, 1969, pp. 157–172.

- [75] L. Kovasznay, Laminar flow behind a two-dimensional grid, in: Mathematical Proceedings of the Cambridge Philosophical Society, Vol. 44, Cambridge University Press, 1948, pp. 58–62.